MILLIMETER ARRAY
MEMO NO. 49

Measurement of Atmospheric Phase Stability with a 225GHz Radiometer

Mark M. McKinnon

May 19, 1988

I. Introduction.

When evaluating potential sites for an array of telescopes operating at millimeter wavelengths, one must understand the phase stability of the atmosphere as well as the atmospheric opacity at each site. Phase stability is typically measured with a multi-element interferometer; however, this experiment attempts to measure phase stability with one of the 225GHz radiometers used in the Millimeter Array site survey. Measuring the phase stability of many sites with a single, portable device is cheaper and logistically simpler than measurements with a multi-element interferometer.

The objectives of this report on the phase stability experiment are:

(1) evaluate the stability of the 225GHz radiometer

(2) illustrate instrumental effects in the collected data and

(3) draw qualitative conclusions regarding phase stability from power spectra and Allan variance.

Although not discussed in this report, the long term objective of the experiment is to correlate the atmospheric phase stability as measured by the radiometer with the phase stability as measured by the VLA.

II. Phase Stability of the Atmosphere.

A. Measuring Phase Stability with an Interferometer.

Consider an interferometer consisting of two radio telescopes operating at millimeter wavelengths. Let the atmosphere above the interferometer be flat, as opposed to curved, with a thickness h. Let the interferometer point at a radio source located at the zenith. In general, the signal from a source is not received simultaneously at each antenna of the interferometer because of the geometry of the interferometer and the signal delay due primarily to atmospheric water vapor*. Since the interferometer under consideration is pointed at zenith, the geometry has no effect on the time delay. To understand phase delay due to the atmosphere, make two simplifying (and incorrect) assumptions:

(1) the atmosphere is stable and

(2) the atmospheric water vapor may be represented by an equivalent thickness of liquid water.

Let the idealized water layer above one antenna have thickness a and the water layer above the other antenna have thickness b. The functional form of the wave propagating in the

* Oxygen also attenuates signals; however, it is thought to be uniformly distributed in the atmosphere so its effect is the same for both antennas.

atmosphere is

$$e^{i(kz-\omega t)} \tag{1}$$

where k is in general complex. For waves propagating in a dissipative medium which is a poor conductor (Jackson),

$$k \simeq \frac{\omega}{c}\sqrt{\mu\epsilon} + i2\pi\sigma\frac{\omega}{c}\sqrt{\frac{\mu}{\epsilon}}. \tag{2}$$

Substituting the expression for k into equation (1), one finds the functional form of the wave to be

$$e^{-2\pi\sigma z\frac{\omega}{c}\sqrt{\frac{\mu}{\epsilon}}}e^{i\frac{\omega}{c}(z\sqrt{\mu\epsilon}-ct)}. \tag{3}$$

The phase of the wave in equation (3) is

$$\phi = \frac{\omega}{c}nz - \omega t \tag{4}$$

since the medium index of refraction, $n = \sqrt{\mu\epsilon}$. After the wave propagates through this hypothetical atmosphere, the phase of the wave at each antenna becomes

$$\phi_1 = \frac{\omega}{c}[(h-a) + na] - \omega t$$

$$\phi_2 = \frac{\omega}{c}[(h-b) + nb] - \omega t$$

where n is now the refractive index of water and the refractive index of air is assumed to be one. The phase delay between the two antennas is

$$\Delta\phi = \phi_2 - \phi_1 = \frac{\omega}{c}[n(b-a) - (b-a)].$$

If δ is the difference in signal path length above the two antennas, then $\delta = b - a$ and

$$\Delta\phi = \omega\delta(n-1)/c = 2\pi\delta(n-1)/\lambda. \tag{5}$$

Equation (5) illustrates the effect of the atmosphere on phase delay, but should not be used for quantitative estimates. The atmosphere is in fact very turbulent, and water vapor is not uniformly distributed in the atmosphere. Turbulence and water vapor concentration determine the index of refraction. The rigorous theoretical treatment of wave propagation in turbulent media and the structure function of refractive index may be found in Tatarski. A concise review of the theory may be found in Thompson et.al.

A straightforward, quantitative estimate of the phase delay due to atmospheric water vapor uses the experimental result of Hogg et.al. They found the radio excess path length due to water vapor, L_v, was related to the total precipitable water vapor, V.

$$L_v = 6.50V \tag{6}$$

Equation (6) is a convenient expression since the total precipitable water vapor may easily be measured. From equation (4), the phase delay due to a change in radio excess path length is

$$\Delta\phi = \omega\Delta(nz)/c = 2\pi\Delta(nz)/\lambda$$

The quantity nz is the radio excess path length. The phase delay then becomes

$$\Delta\phi = 2\pi\Delta L_v/\lambda = 13\pi\Delta V/\lambda. \quad (7)$$

The phase stability of an atmosphere is poor if the magnitude of $\Delta\phi$ is large. Phase stability is both a function of time and antenna spacing. The phase stability at large spacings is likely to be worse than at short spacings since the atmosphere is more likely to change over large distances.

B. Measuring Phase Stability with a Single Radiometer.

The 225GHz radiometer used in the Millimeter Array site survey subtracts a reference temperature, T_{cr}, from a signal temperature, T_s, (McKinnon).

$$T_s = T_r + T_1(1-\epsilon) + T_A(1-e^{-\tau})$$

$$T_{cr} = T_r + T_1(1-\epsilon) + \epsilon T_c$$

$$T_s - T_{cr} = T_A\epsilon(1-e^{-\tau}) - \epsilon T_c$$

T_r is the receiver temperature, T_1 is the temperature at which losses are terminated, ϵ is the coupling efficiency, T_c is the physical reference temperature, and τ is the atmospheric opacity at zenith. Here, background sources such as the microwave background radiation have been assumed to be negligible. The expressions for the temperatures are derived from the radiative transfer equation for a constant source function in the Rayleigh-Jeans limit. The radiometer synchronous detector voltage, V, is proportional to the temperature difference

$$V = GT_A(1-e^{-\tau}) - GT_c$$

where $G = \epsilon g$ is the radiometer gain and g is the constant of proportionality. Therefore the brightness temperature of the atmosphere as detected by the radiometer is

$$T_b = V/G + T_c = T_A(1-e^{-\tau})$$

and the opacity is

$$\tau = -ln(1 - T_b/T_A).$$

As the atmosphere moves over the radiometer, the radiometer brightness temperature will change because the opacity varies. The fluctuation in opacity is then

$$\Delta\tau = \tau_2 - \tau_1 = ln\left[\frac{T_A - T_{b1}}{T_A - T_{b2}}\right]. \tag{8}$$

The atmospheric opacity is related to the millimeters of precipitable water vapor, V, by

$$\tau = \beta V$$

where β is a constant of proportionality dependent upon observing wavelength. Therefore the opacity fluctuations are related to the difference in path lengths for different brightness temperature measurements.

$$\Delta\tau = \beta\Delta V \tag{9}$$

The corresponding change in phase, in radians, may be found using equations (7), (8), and (9).

$$\Delta\phi = \frac{13\pi\Delta\tau}{\beta\lambda} = \frac{13\pi}{\beta\lambda} ln\left[\frac{T_A - T_{b1}}{T_A - T_{b2}}\right].$$

For the radiometers used in the Millimeter Array site survey, the change in phase is

$$\Delta\phi(\text{degrees}) = 29,323 ln\left[\frac{265 - T_{b1}}{265 - T_{b2}}\right]. \tag{10}$$

Equation (10) was generated using $\lambda = 1.33$mm, $\beta = 0.06$ nepers/mm, and $T_A = 265$K. Figure 1 is a plot of the time series data for an atmosphere stability run conducted on March 18, 1988 at the VLA. The temperature units are degrees Kelvin absolute. The run consists of 1024 data points taken at 3.5 second intervals. Each data point is the average of seven separate data points collected during the 3.5 second interval. During the run, the sky was clear, the wind speed was 1.2 m/s, and the ambient temperature ranged from 7 to 10C. The increase in ambient temperature is evident in the gradual increase of temperature in the data. The brightness temperature at about 500 samples changes from 77K to 67K. Using equation (10), the corresponding change in phase would be $1,520°$.

When the atmosphere is optically thin ($\tau << 1$), the opacity is

$$\tau \approx T_b/T_A$$

and the fluctuation in opacity is

$$\Delta\tau = \Delta T_b/T_A = (\tau_2 T_A - \tau_1 T_A)/T_A.$$

The change in phase which corresponds to the fluctuation in opacity is

$$\Delta\phi = \frac{13\pi\Delta T_b}{\beta\lambda T_A}.$$

For the 225 GHz radiometer, the change in phase in the optically thin case is

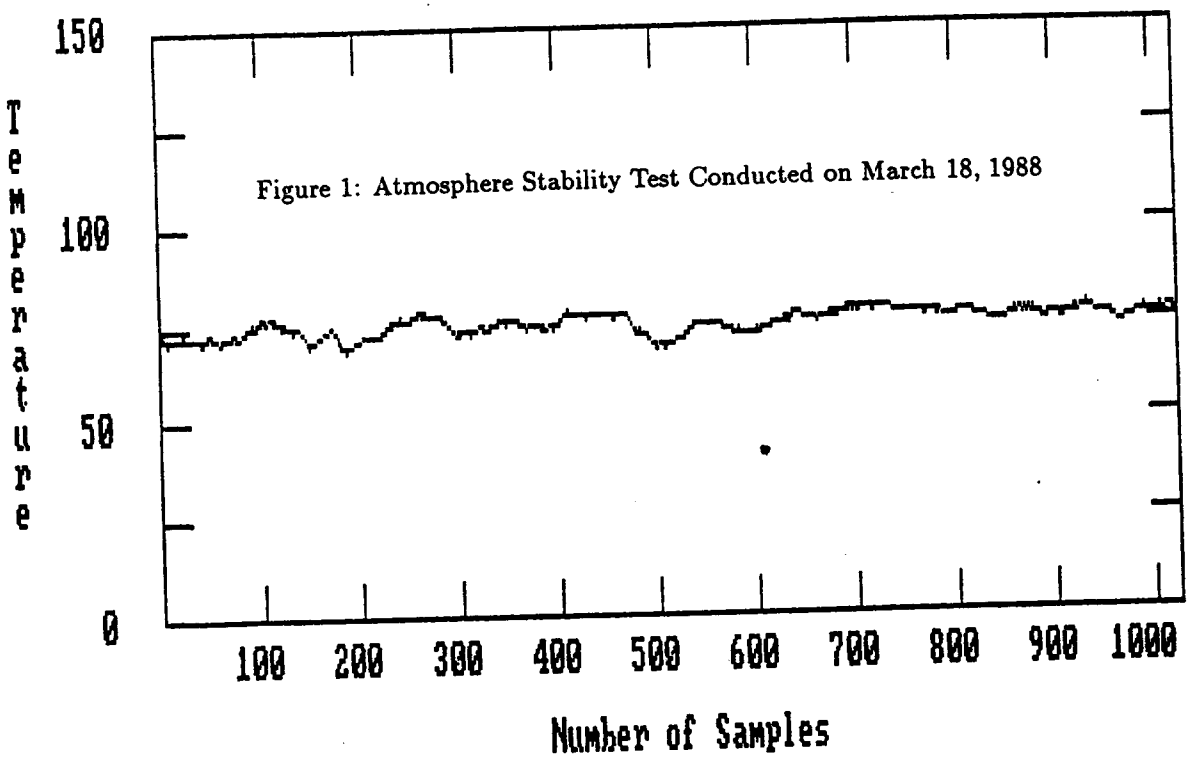

Figure 1: Atmosphere Stability Test Conducted on March 18, 1988

File: 88031802.phi

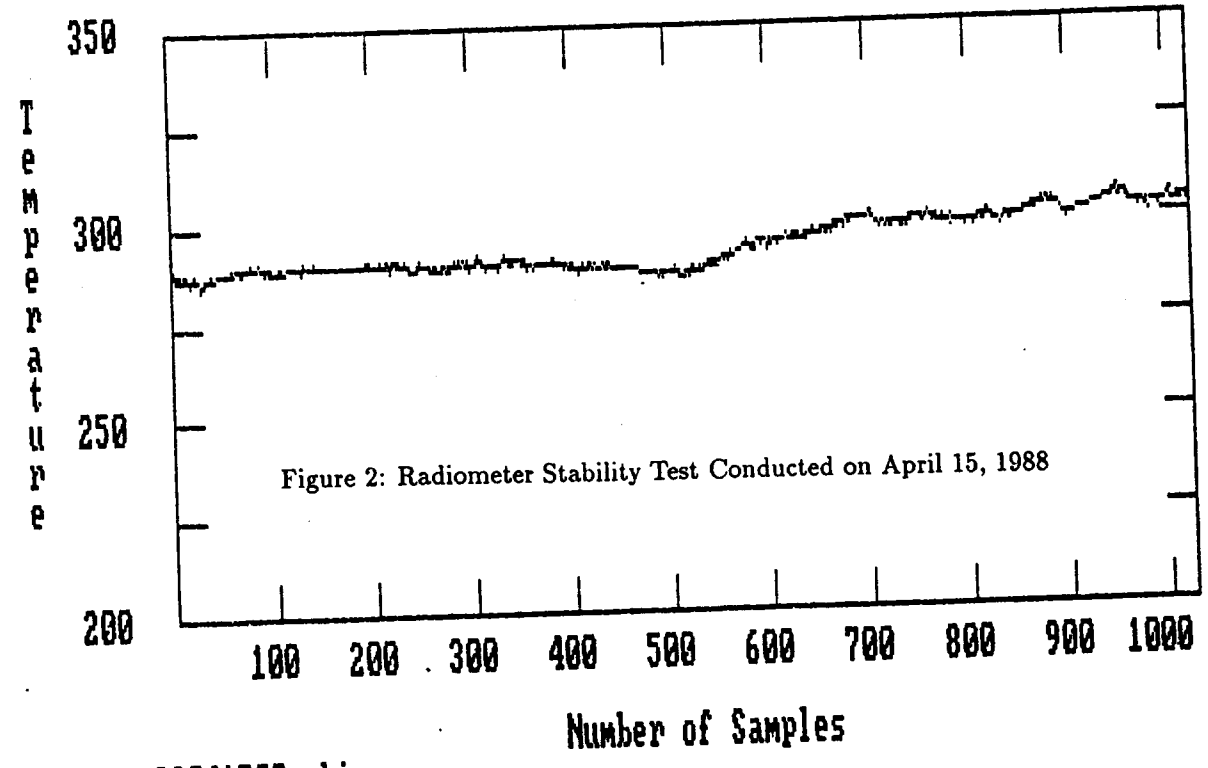

Figure 2: Radiometer Stability Test Conducted on April 15, 1988

File: a:88041500.phi

$$\Delta\phi(\text{degrees}) = 110\Delta T_b(\text{K}). \tag{11}$$

Data in other atmosphere test runs appear to be very stable with an rms of 1.5K. The corresponding phase delay for an optically thin atmosphere with uncorrelated fluctuations is $110 \times 1.5\sqrt{2} = 233°$. This phase delay is due to the long term variation in opacity over the one hour duration of the test. Short timescale phase changes in the same data set would be much less than 233°. It is also possible that the fluctuations are correlated so that the corresponding phase delay is actually an upper limit. One should use caution in applying equation (11) since the parameters discussed later in this report indicate atmospheric fluctuations are dominant only at intermediate timescales (30 sec $< t <$ 10 min).

III. Radiometer Stability.

Before analyzing phase stability measurements, questions regarding the stability of the radiometer must be answered. Is the radiometer stable enough to measure atmospheric fluctuations? Do the radiometers agree with one another when measuring the fluctuations?

A. Radiometer Stability Tests and Effects of the Sun.

The radiometer stability was tested by placing absorber over the radiometer external mirror and collecting data for the duration (one hour) of a normal phase stability run. In this configuration, the radiometer measures the ambient temperature. The absorber cannot be placed directly over the mylar window because the absorber equilibriates with the radiometer internal temperature (45C) instead of ambient temperature. A plot of radiometer test data converted to absolute temperature is shown in Figure 2. The radiometer was located on top of the VLA control building, and the data collection began at 0920MST on April 15 for this particular data set. The ambient temperature, which can be monitored by the radiometer, was 16C at 0920 and was 18C one hour later. With the exception of the large rise in measured temperature, the data seem very reasonable. The noise in the data is consistent with the radiometer's theoretical sensitivity (0.13K for 3.5 second integration times). The measured temperature at the beginning of the run is consistent with ambient temperature. The measured temperature at the end of the run is much higher than ambient. The temperature rise is caused firstly by detection of the Sun and secondly by heating of the control building which reradiates into the absorber covered mirror. To verify the preceding statement, the same test was performed early in the morning on April 22, 1988. The data from three successive runs on April 22 are shown in Figures 3, 4, and 5. The starting time for each run was 0524, 0635, and 0744 MDST, respectively. Sunrise occurred at about 0630. The actual ambient temperature was monitored with the VLA weather station during the tests. The actual ambient temperatures are plotted as straight, solid lines in the figures. The disturbing feature in the figures is the noise in the radiometer data. The tests conducted on March 18, April 15, and April 22 used the same radiometer. Apparently the radiometer's performance degraded between the last two days of testing. Note as actual ambient temperature increases, the radiometer noise decreases. The noise is indirectly caused by temperature gradients in the radiometer enclosure. Radiometer components which are not located in the vicinity of the enclosure heater are adversely affected by the temperature gradient. Subsequently, the components

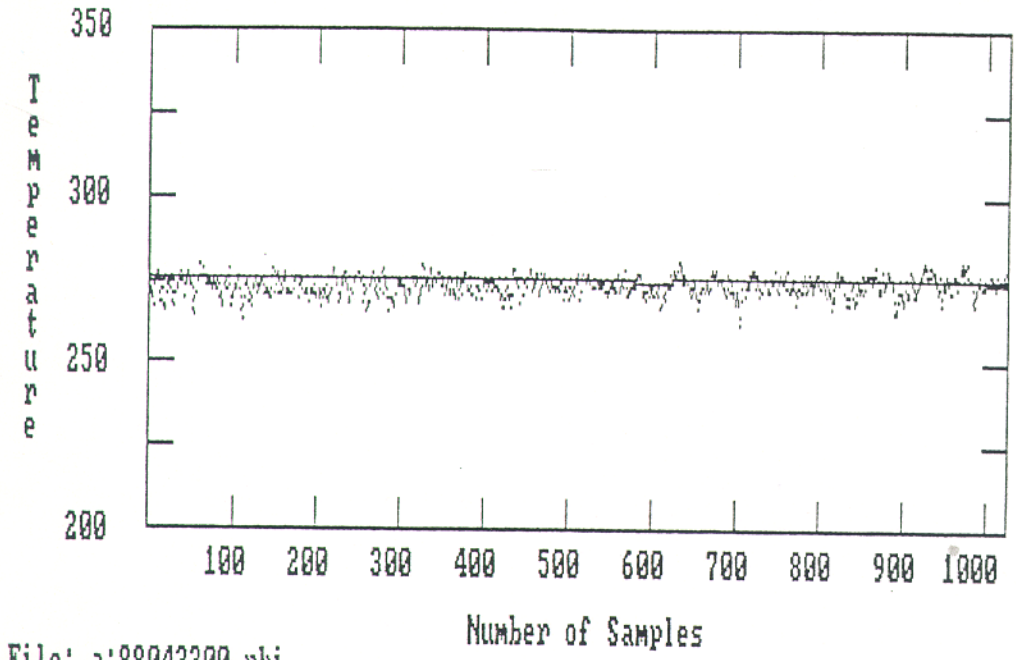

Figure 3: Radiometer Stability Test
April 22, 1988, 0524 MDST

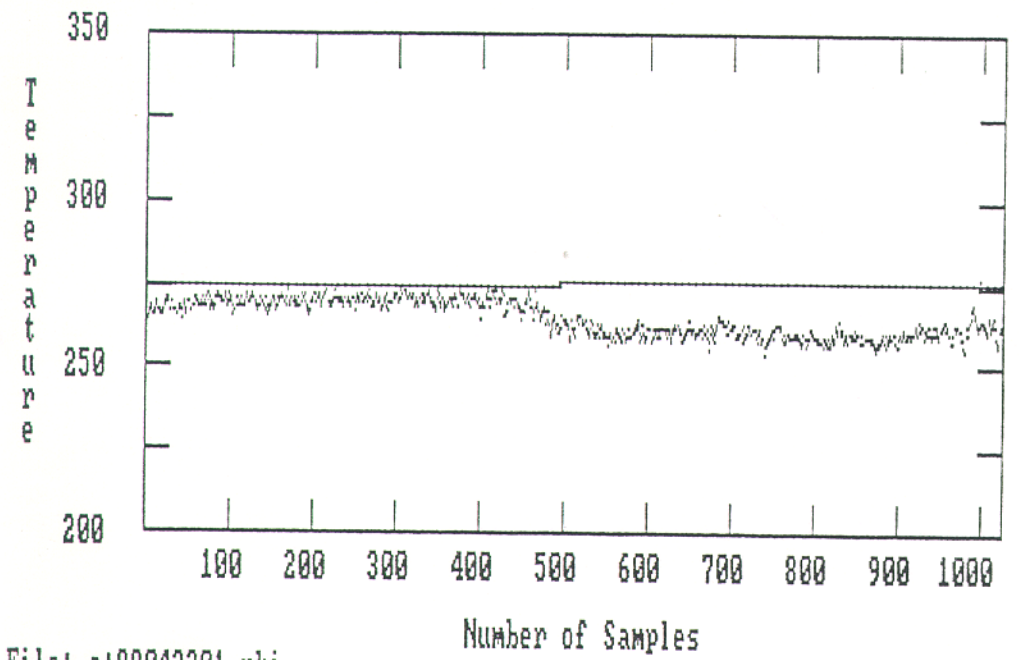

Figure 4: Radiometer Stability Test
Aprill 22, 1988, 0635 MDST

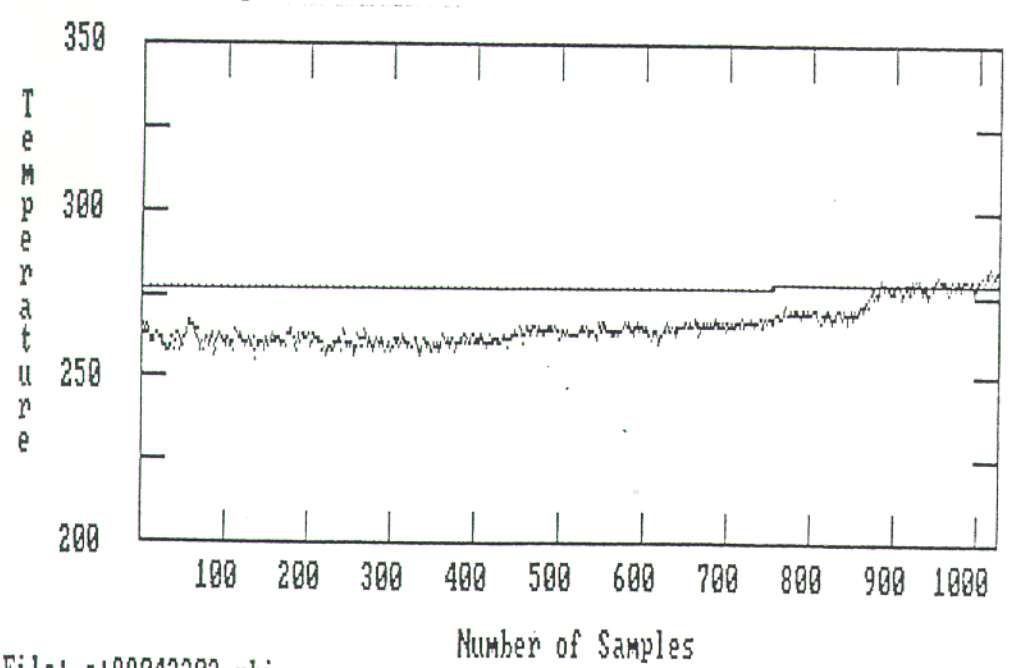

Figure 5: Radiometer Stability Test
April 22, 1988, 0744 MDST

may not be operating in their design temperature range. The mixer is the component most suspectible to this problem. It is located further from the heater than any other component. The mixer current changed from 0.150 ma at the start of the test runs to 0.257 ma at the end of the test runs. The normal mixer current is 0.250 ma. The gunn oscillator and tripler currents remained essentially constant over the same time period. Although the mixer is not operating ideally in these runs, it is still operational. One may still analyze the results for additional information.

The gratifying feature in Figure 3 is the long term stability of the radiometer. The actual ambient temperature during this run hardly changed. With the exception of the noise, the radiometer output remained essentially constant over the same time period. The difference between actual and measured ambient temperature corresponds to an error of about three percent. The error arises primarily from inaccuracies in calibrating the radiometer. A less likely cause for the error is the absorber is not an ideal blackbody. This implies the absorber is at least 97% efficient in reradiating its incident radiation. The data in Figures 4 and 5 were affected by the Sun. Suprisingly, the temperature measured by the radiometer *decreased* after sunrise. The measured temperature then increased above ambient at the conclusion of the third test. A possible explanation for this effect is evaporation of water from the absorber. The absorber cooled as the water evaporated until no water concentration gradient existed between the absorber and the air. Then the absorber began to warm as the local ambient temperature increased. Although the ambient temperature at the VLA weather station remained essentially constant, the ambient temperature recorded at the radiometer was 1.2C at 0624 and 9.6C at 0844.

B. Radiometer Comparison.

Figures 6a, 6b, and 6c are plots of sky brightness temperature as measured by radiometer Nos.1, 3, and 4, respectively. All three figures are plotted on the same relative temperature scale. The measurements by radiometers No.1 and No.3 started simultaneously, and the measurements by radiometer No.4 started about two minutes later. The plots qualitatively show that all three radiometers performed similarly in measuring the sky brightness temperature. The relatively large change in brightness temperature at the left of the figures serves as a good reference for comparing other fluctuations in the figures. It appears that sky fluctuations are detected simultaneously by all three radiometers. The apparent noise in the data for radiometers No.1 and No.3 was due to a software error, which has been corrected. The noise in the radiometer No.4 data was caused by the same software error and the impending failure of the local oscillator.

C. Gain Averaging.

A subtle point regarding the analysis of the time series data is gain averaging. Each data point is corrected for the radiometer gain. While the gain monitor detects the 20C difference between the hot load temperature and the cold load temperature, the signal detector measures the difference between the brightness temperature and the cold load temperature. The difference between brightness temperature and cold load varies. The fluctuation in the gain measurement is

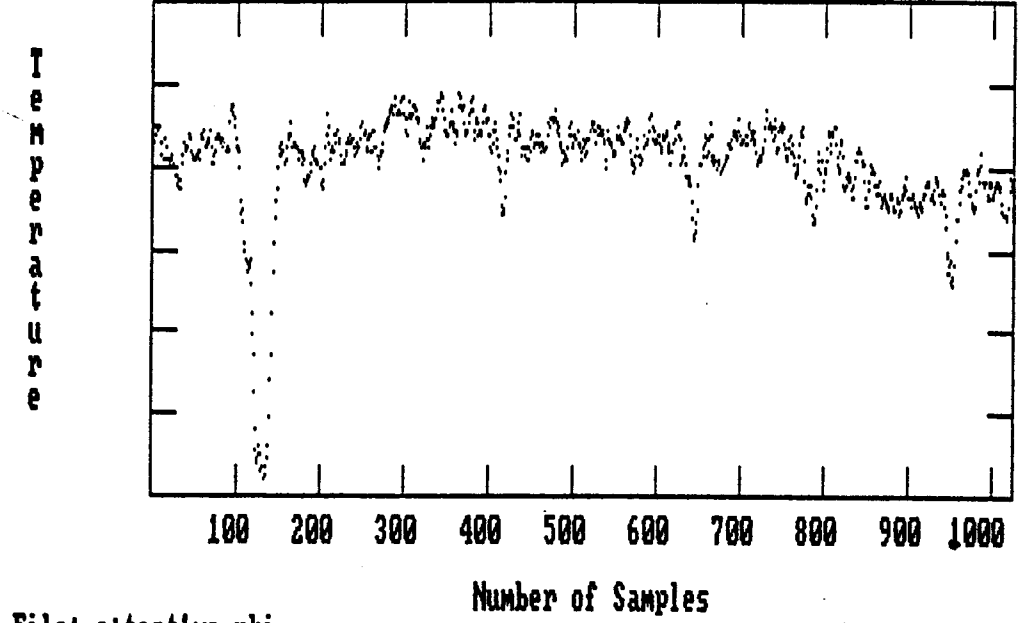

Figure 6a: Atmosphere Stability Test
Radiometer No.1, March 17, 1988

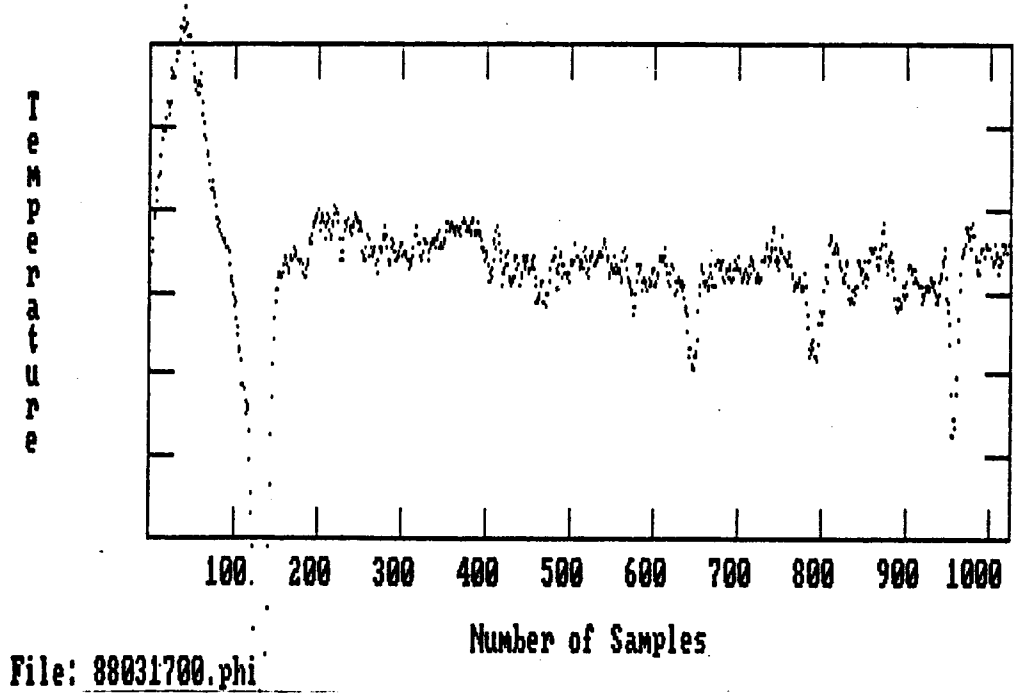

Figure 6b: Atmosphere Stability Test
Radiometer No.3, March 17, 1988

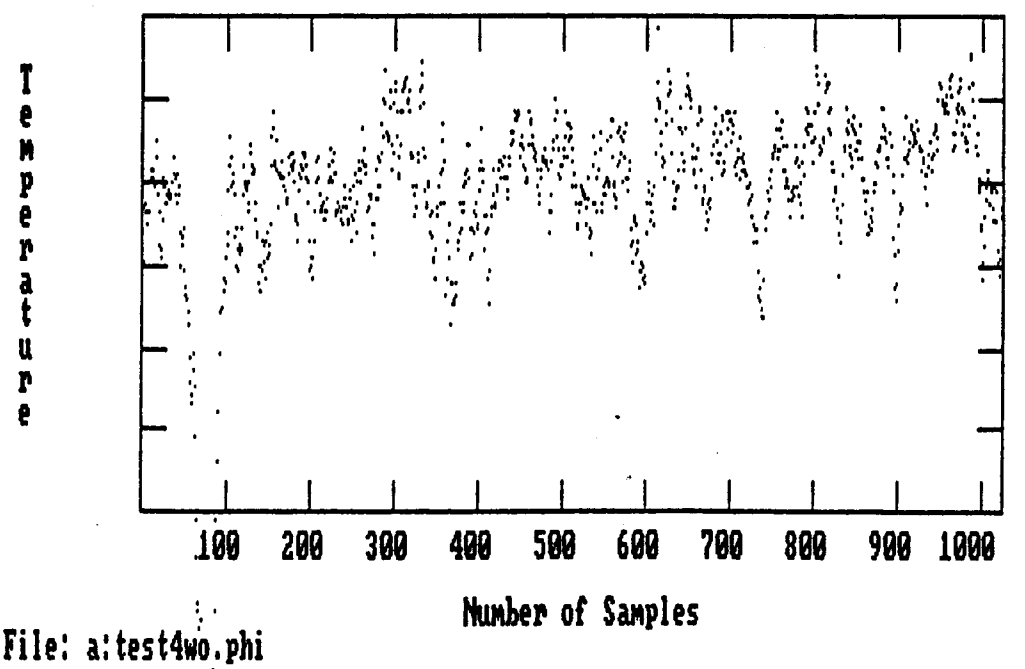

Figure 6c: Atmosphere Stability Test
Radiometer No.4, March 17, 1988

$$\sigma_g = \frac{\Delta T_g}{T_g} = \frac{K T_{sys}}{20\sqrt{\Delta\nu\tau_g}} \tag{12}$$

and the fluctuation in the signal measurement is

$$\sigma_s = \frac{\Delta T_s}{T_s} = \frac{K T_{sys}}{T_s\sqrt{\Delta\nu\tau_s}} \tag{13}.$$

In order to correctly measure the signal fluctuation, the gain fluctuation cannot exceed the signal fluctuation. By equating equation (12) to equation (13), the gain monitor integration time must be

$$\tau_g = \left(\frac{T_s}{20}\right)^2 \tau_s \tag{14}$$

since the system constant, K, the detection bandwidth, $\Delta\nu$, and the system temperature, T_{sys}, are the same for both detector circuits. Both the signal and gain are effectively sampled at 3.5 second intervals in this experiment; therefore, the gain must be averaged for a large number (N) of data points for the equality in equation (14) to remain true. In other words, each data point is not corrected concurrently for gain, but is corrected after data collection with an average gain. Since $\tau_s = 3.5$ seconds and $\tau_g = 3.5N$ seconds, the number of successive gain data points to average is

$$N = (T_s/20)^2.$$

Note that during a radiometer stability test, T_s is the difference between ambient temperature ($\sim$ 25C) and cold load temperature (45C). This means gain averaging has no effect on a radiometer test because N is one. However, during an atmosphere stability test, T_s may be as large as 300, so N must be 225. As a matter of convenience, all data is currently processed with $N = 256$. The effect of gain averaging is shown in Figures 7a and 7b. Figure 7a is a data set with gain applied concurrent with data collection. Figure 7b is the same data set with the gain averaged and applied after data collection. It is obvious from the figures that the apparent noise is reduced by applying gain averaging. Gain averaging was not applied to Figures 6a through 6c because the data from these runs was not in the raw form required for the gain averaging technique.

IV. Allan Variance as an Indicator of Stability.

Allan variance is typically used to measure the stability of a local oscillator or frequency standard. This experiment uses Allan variance to make qualitative estimates of the stability of the radiometers and the atmosphere. The two sample Allan variance for zero dead time between measurements is given by

$$\sigma_A \simeq \frac{1}{2(M-1)} \sum_{k=1}^{M-1} (\bar{y}_{k+1} - \bar{y}_k)^2$$

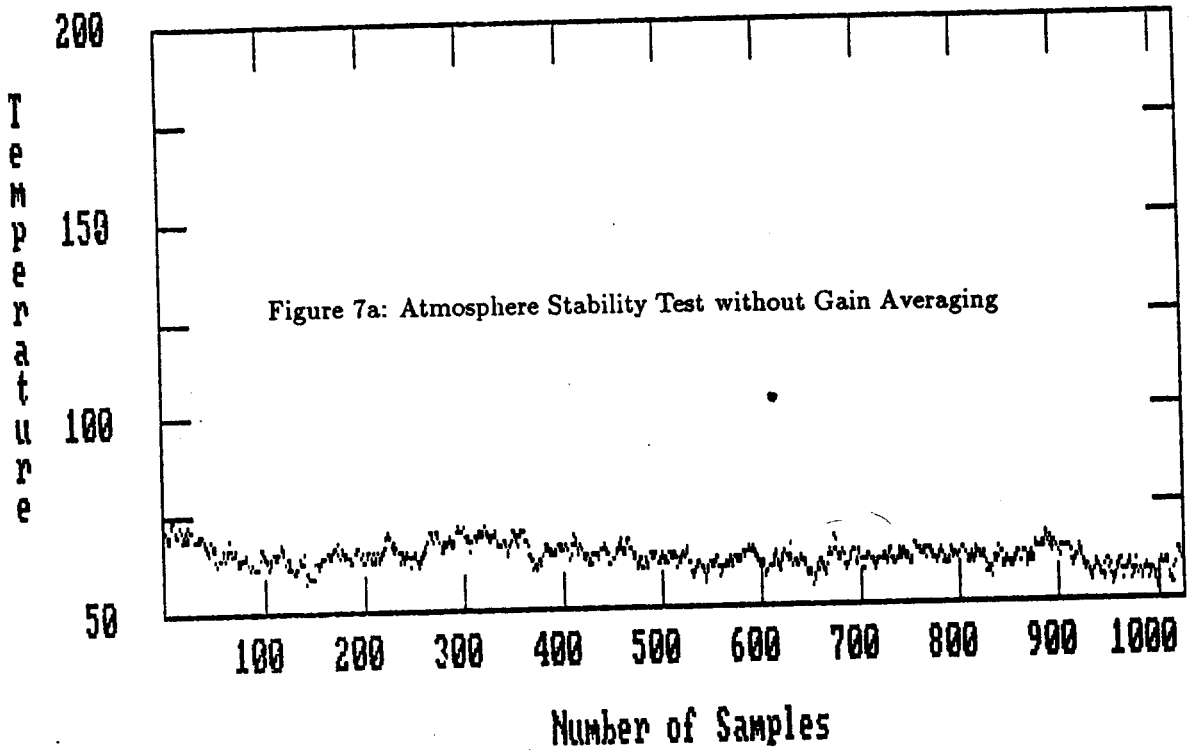

Figure 7a: Atmosphere Stability Test without Gain Averaging

File: a:88040800.phi

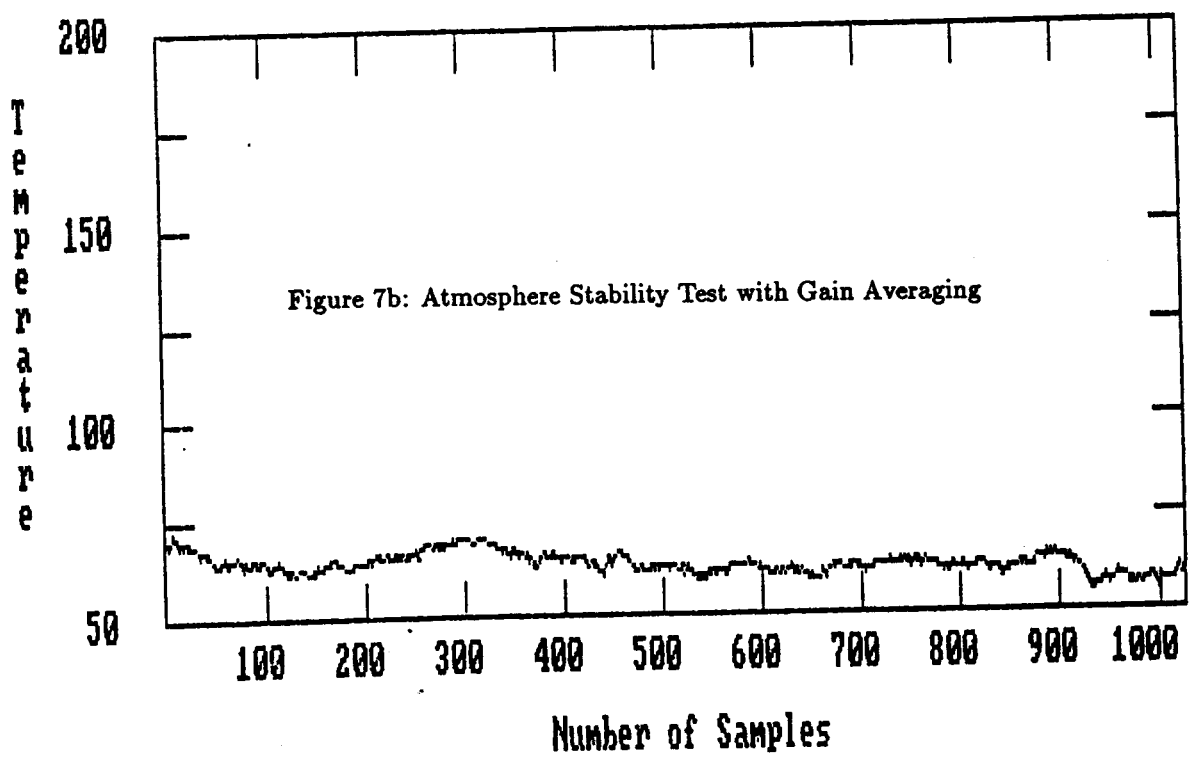

Figure 7b: Atmosphere Stability Test with Gain Averaging

File: a:88040800.phi

where M is the number of data points. The bar over the y indicates that y has been averaged over a certain time interval. The Allan variance at longer time intervals may be computed from the same data set by dividing the data set into subsets and averaging successive data points within the subset. Data sets or subsets with large Allan variances are not as stable as those with small Allan variances.

When applying the Allan variance to a radiometer stability run and an atmosphere stability run, what should one expect? If a radiometer is performing correctly, the Allan variance for a radiometer test (absorber over the mirror) should not change much with different time intervals. From the the atmosphere test, the product of wind velocity and elapsed time, $v_w t$, may be used to estimate an interferometer antenna spacing. Therefore rapid fluctuations (phase changes) which obviously occur at short timescales will be measured by short baselines. Long baselines will measure rapid *and* slow fluctuations. The magnitude of the fluctuations will depend upon the characteristics of the atmosphere. Also, as stated in section II, the phase stability at large antenna spacings is worse than at short antenna spacings. Then one might expect the Allan variance, in general, to increase with increasing timescales. These expectations are basically confirmed in Figures 8a through 9b. Figures 8a and 8b are plots of the time series data and Allan variance, respectively, for a radiometer stability test run. Figures 9a and 9b are plots of the time series data and Allan variance for an atmosphere stability run. The Allan variance plot for the radiometer stability test is flat except for the increase in variance at large timescales. The increase might be due to the long term change in ambient temperature during the test run. The Allan variance for the atmosphere stability test behaves as expected except for the abrupt decrease in variance at large timescales. Intermediate timescale events are dominated by atmospheric fluctuations. Notice that the magnitudes of the Allan variance at small timescales are similar for both Allan variance plots. The same may be said for large timescales. These facts imply that short timescale phenomena are dominated by the radiometer while large timescale events might be dominated by fluctuations in ambient temperature during the test runs. Smoot et.al. also found short timescale phenomena to be dominated by instrumental effects.

The Allan variance at *intermediate* timescales may then be used to quantitatively estimate phase stability using equation (11). The most stable atmosphere tests of the VLA site to date have Allan variances of 0.0725 at timescales of 3.7 minutes. Equation (11) implies the upper limit on phase stability is $110\sqrt{2 \times 0.0725} = 42°$. The phase stability at a different wavelength may be calculated by multiplying the measured phase stability by the wavelength ratio e.g. the phase stability at 1.3cm corresponding to 42° at 225GHz (1.3mm) is 4.2°.

V. Phase Stability and the Spectrum of Turbulence.

From Smoot et.al. and Ulich, the Kolmogorov power spectrum of atmospheric turbulence, as traced by fluctuations in atmospheric water column density, is given by

$$|P(\Delta V)|^2 = C^2 \nu^{-5/3} D^{2/3} \tag{15}$$

where C is a normalization constant, D is the horizontal distance scale, and ν is the

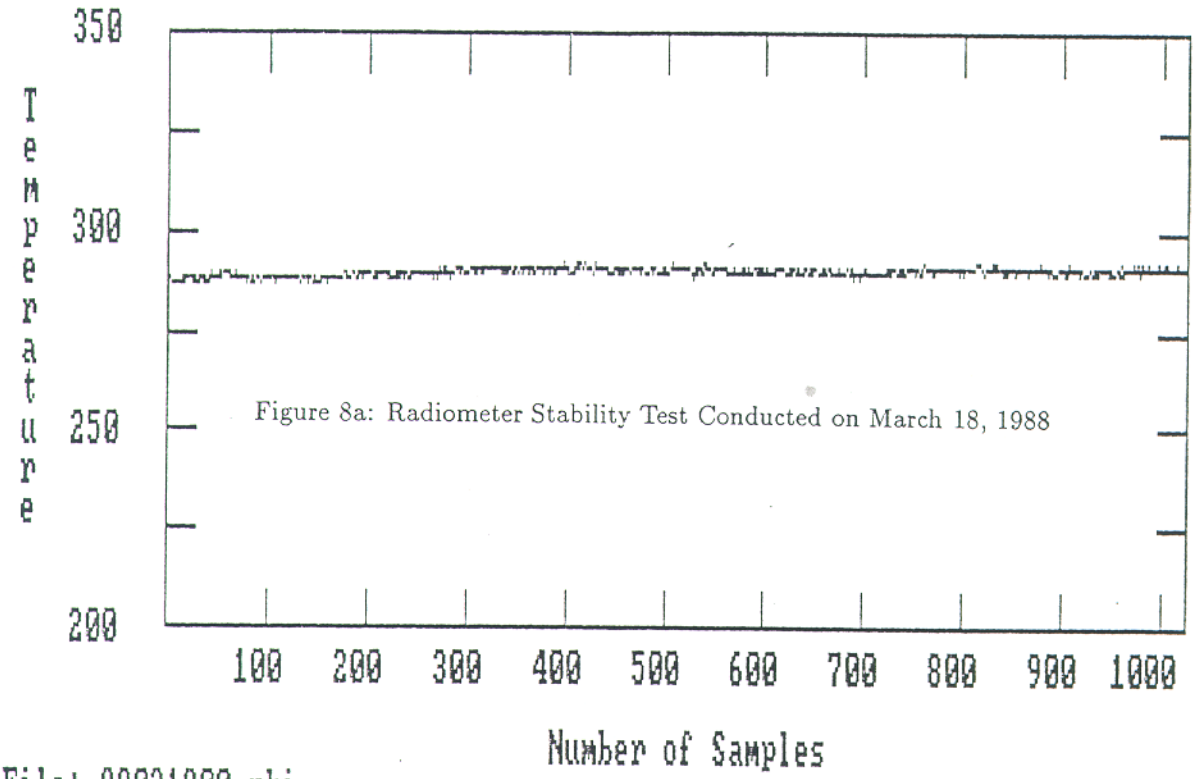

Figure 8a: Radiometer Stability Test Conducted on March 18, 1988

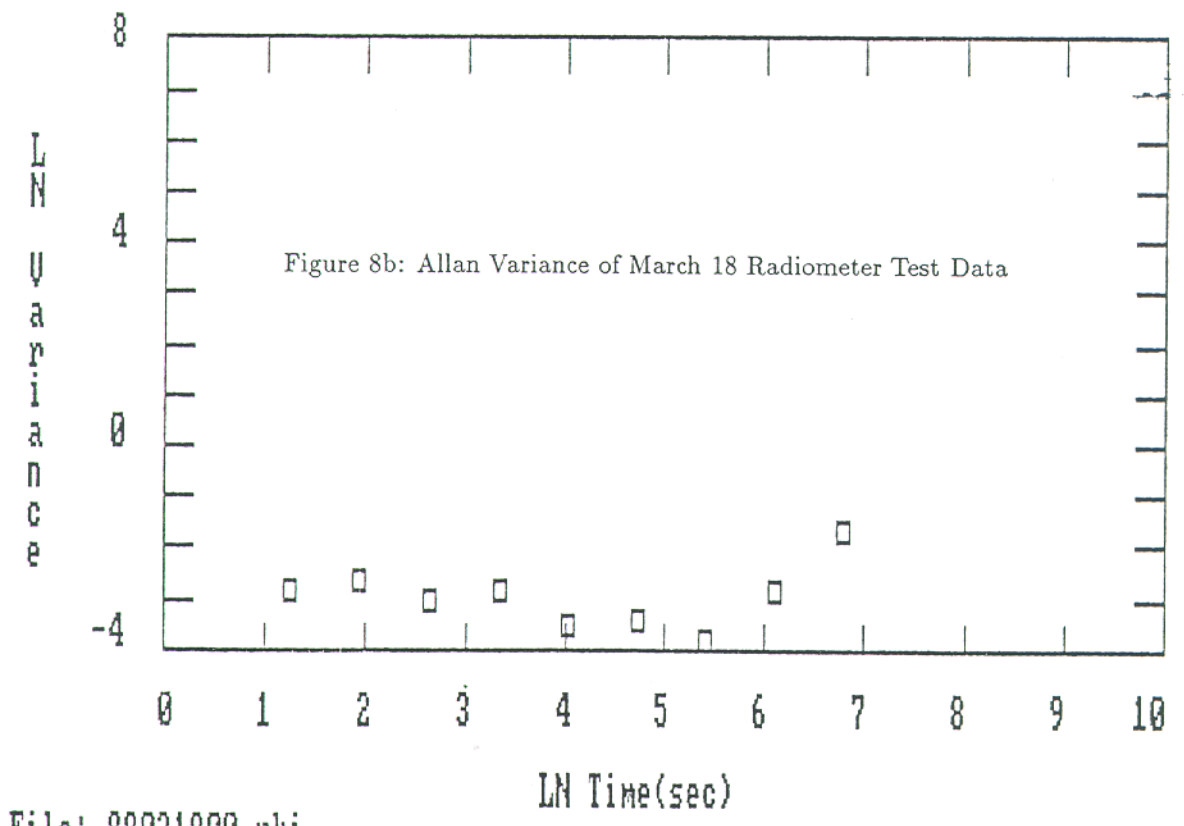

Figure 8b: Allan Variance of March 18 Radiometer Test Data

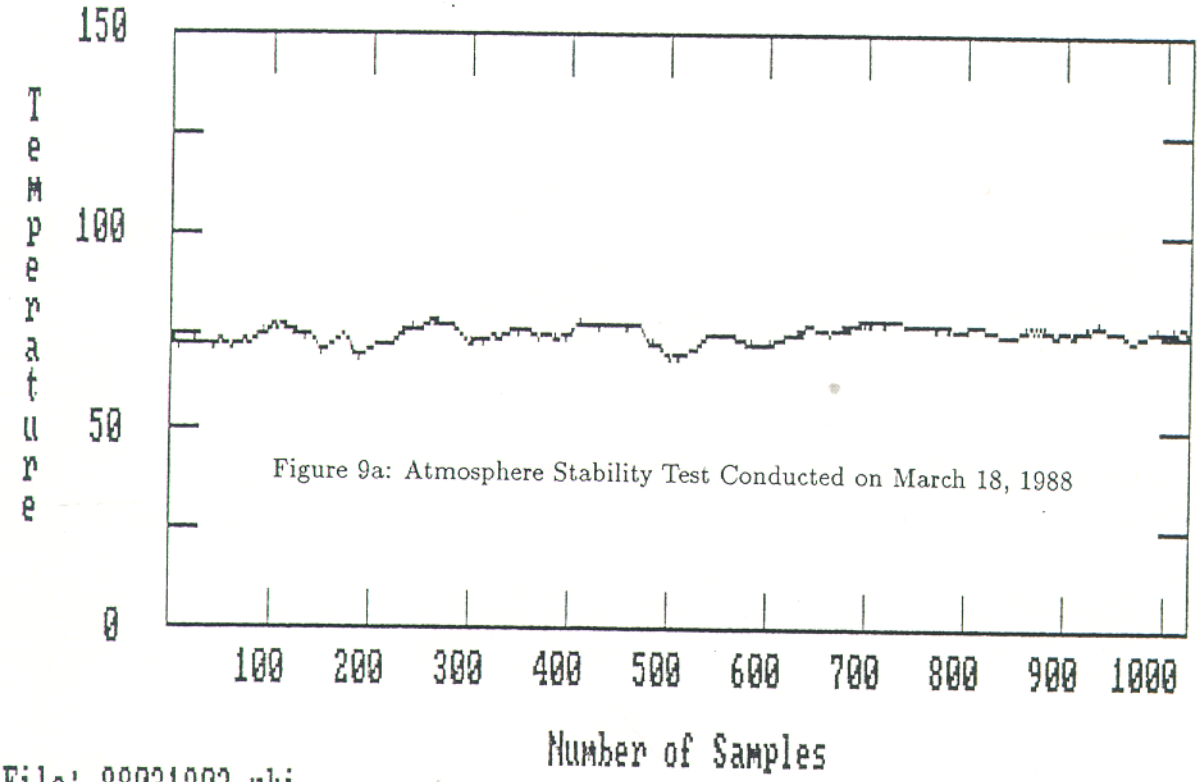

Figure 9a: Atmosphere Stability Test Conducted on March 18, 1988

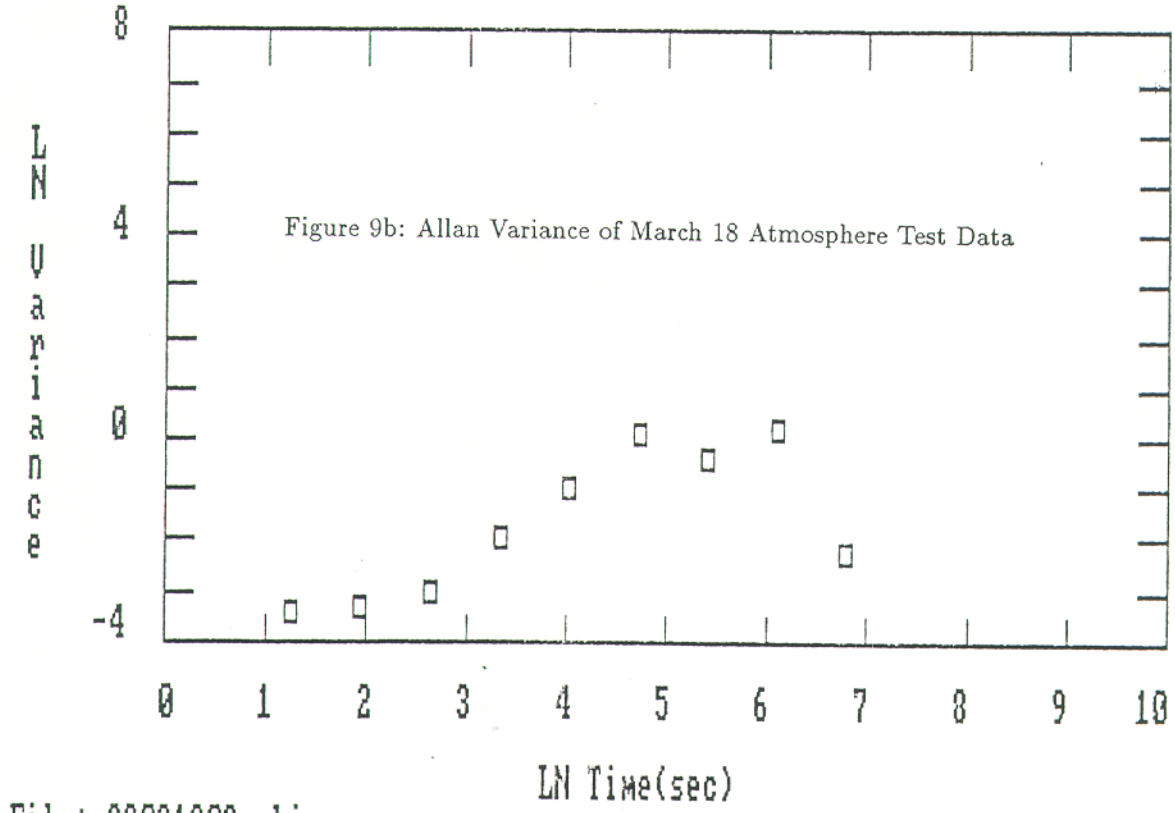

Figure 9b: Allan Variance of March 18 Atmosphere Test Data

frequency. The horizontal distance scale for the radiometer is the product of the wind velocity and the duration of the measurement, $v_w t$. If one applies equation (15) to the radiometer time series data, the power spectrum should have a slope of $-5/3$ in frequency. When comparing two spectra from different stability runs, the data set which represents a more turbulent atmosphere should have more power in its spectrum.

Figure 11 is the power spectrum of the data in an atmosphere stability test conducted on September 25, 1987. The spectral index, 1.55 ± 0.06, is similar to that predicted by the Kolmogorov turbulence model, 1.67. The spectral index was found by performing a least squares analysis on the power spectrum data.

Figure 10a is the power spectrum generated by taking the Fourier transform of the radiometer test data in Figure 8a. Figure 10b is the power spectrum of the atmosphere test data in Figure 9a. The smallest frequency in the spectra is determined by the duration of the test, and the largest frequency is determined by the Nyquist frequency ($1/2\Delta t$). The spectra appear clumped at large frequencies because they are log-log plots. Although difficult to see, the atmosphere test spectrum is steeper than the radiometer test spectrum. The power at intermediate frequencies is larger in the atmosphere test spectrum than the radiometer test spectrum. At large frequencies (short timescales) the magnitude of the power in both spectra is comparable. The power of the isolated data points at short frequencies (long timescales) is also comparable in both spectra. In summary, the spectra are restating what was found with Allan variance: (1) short timescale events are dominated by the instrument and (2) long timescale events might be dominated by long term variations in ambient temperature.

The power spectra may be used to determine phase stability in the following manner. Select a data set which has acceptable phase stability. What is acceptable may be determined by a VLA test run or by applying equation (11) to the rms of a data set. Choose a horizontal distance scale (baseline) of interest, say one kilometer, and calculate a timescale with the equation $D = v_w t$. An acceptable power level may be determined with the power spectrum using the frequency which corresponds to the calculated timescale. The power level determined at the same baseline from subsequent stability tests may be compared to the acceptable power level to decide if the atmosphere was 'phase stable' during the test. Data sets with excessive spectral power are more turbulent or 'phase unstable'.

VI. Conclusions.

Radiometer measurements of the atmosphere give reasonable results. The radiometer brightness temperature is consistent with the product of an opacity and atmosphere temperature in the optically thin limit. The Allan variance and power spectra used to analyze the data give consistent results. Intermediate frequencies and timescales in atmosphere test data have large power and variance for data sets with large brightness temperature rms. Short timescale measurements are dominated by the instrument. From currently available data, the upper limit on the phase stability at the VLA site at 225 GHz is at best 42° for timescales of 3.7 minutes. The phase stability at slightly shorter timescales could be better. Now that the radiometer time series data is better understood, radiometer atmosphere tests may be compared with VLA test runs to search for a radiometer/VLA phase stability correlation.

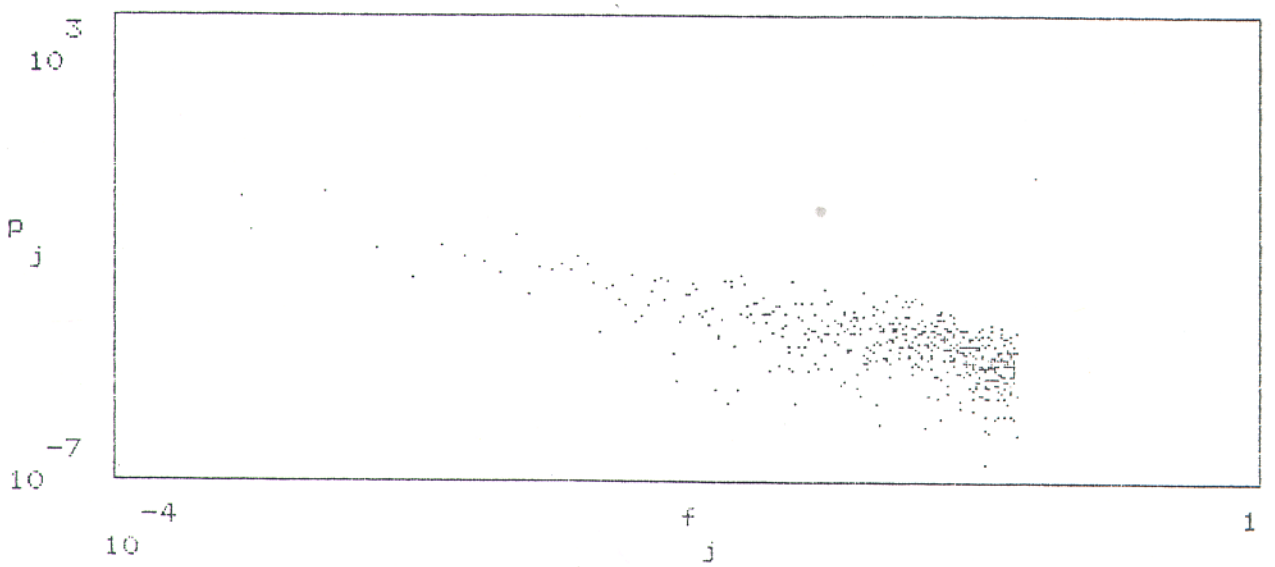

Figure 10a: Power Spectrum of March 18 Radiometer Test Data

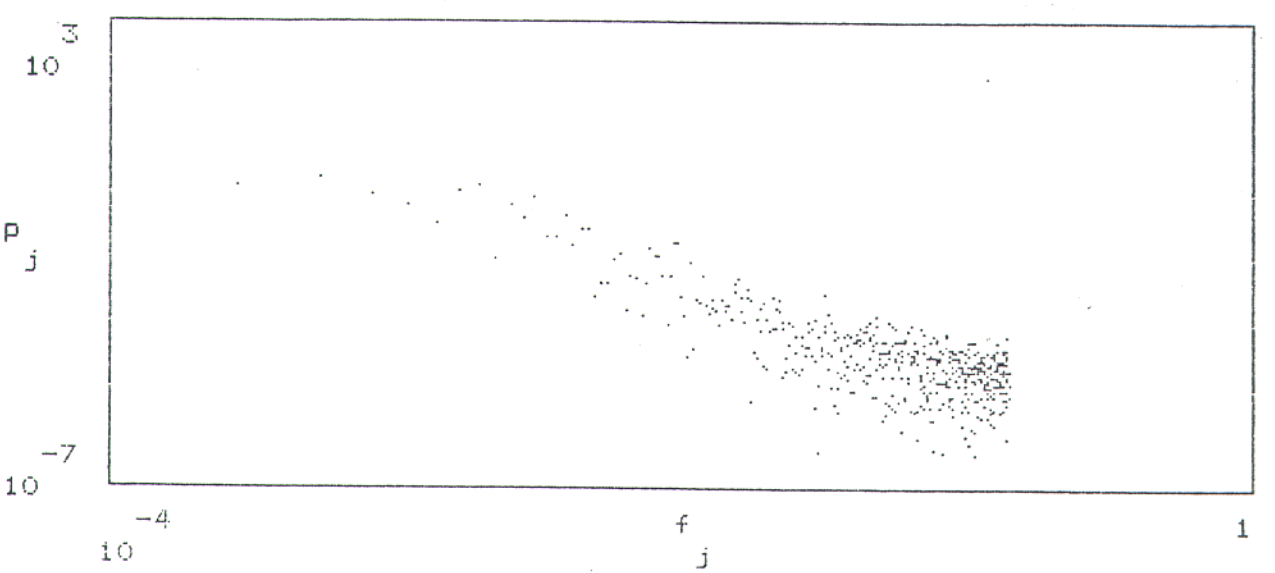

Figure 10b: Power Spectrum of March 18 Atmosphere Test Data

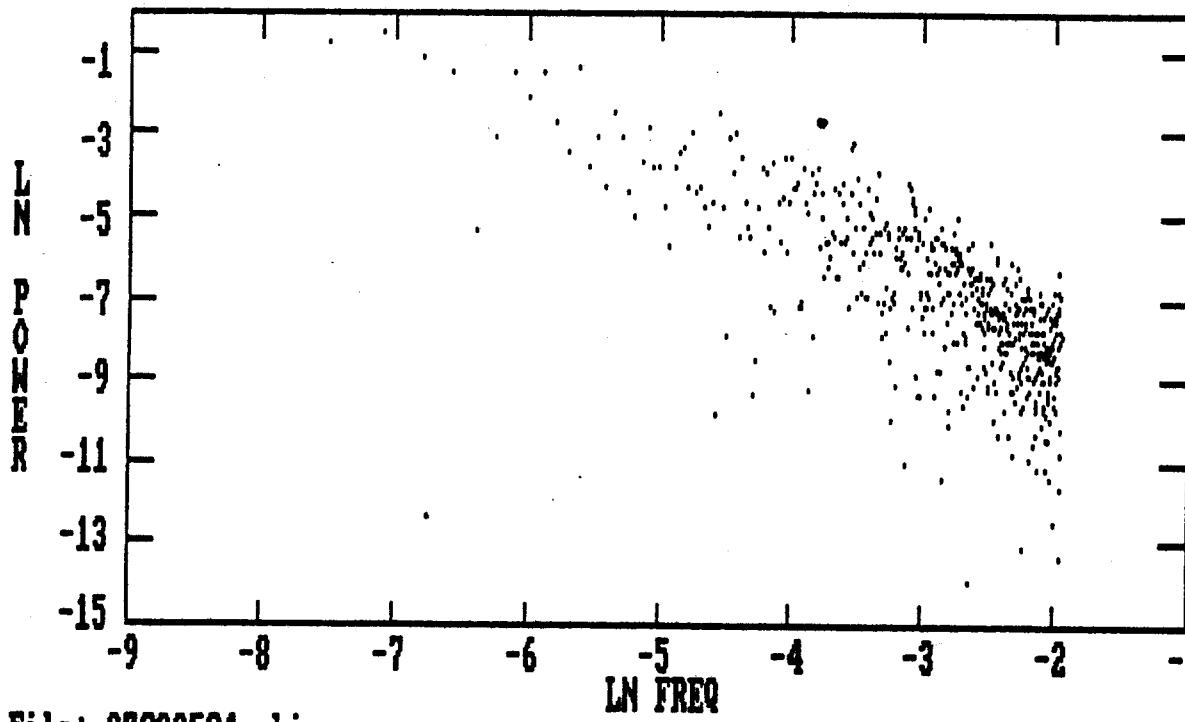

Figure 11: Power Spectrum of September 25, 1987 Atmosphere Test Data

References.

Blair, B.E., 1974, Time and Frequency: Theory and Fundamentals, National Bureau of Standards Monograph 140, U.S. Government Printing Office, Washington, D.C.

Bracewell, R.N., 1986, The Fourier Transform and Its Applications, McGraw-Hill Book Company, New York.

Hogg, D.C., Guiraud, F.O., and Decker, M.T., 1981, Astron. Astrophys., 95, 304-307.

Jackson, J.D., 1975, Classical Electrodynamics, John Wiley and Sons, New York.

McKinnon, M.M., 1987, Millimeter Array Memo. No.40.

Tatarski, V.I., 1961, Wave Propagation in a Turbulent Medium, McGraw-Hill Book Company, New York.

Thompson, A.R., Moran, J.M., and Swenson, G.W., 1986, Interferometry and Synthesis in Radio Astronomy, John Wiley and Sons, New York.

Smoot, G.F., Levin, S.M., Kogut, A., De Amici, G., and Witebsky, C., 1987, Radio Science, 22(4), 521-528.

Sramek, R.A., 1983, VLA Test Memo. No.143.

Ulich, B.L., 1984, Millimeter Array Memo. No.15.

Appendix A: Ringing in Power Spectra

Figures 12a through 13b display the hazards of blindly applying the Fourier transform. Figures 12a and 13a are the data from atmosphere stability test runs conducted on September 14 and 15, 1987, respectively. The power spectra of the data are shown in Figures 12b and 13b. The sinusoidal components in the spectra, called ringing, are caused by the large, abrupt decreases in brightness temperature in the time series data. The large, abrupt decreases may be thought of as delta functions, and the ringing results from the shift in the Fourier transform of a delta function. The delta function may be represented by a combination of the functions

$$f(x) = \frac{1}{2}\delta(x + 1/2) + \frac{1}{2}\delta(x - 1/2)$$

$$g(x) = \frac{1}{2}\delta(x + 1/2) - \frac{1}{2}\delta(x - 1/2)$$

which have the Fourier transforms

$$f(x) \supset \cos \pi s$$

$$g(x) \supset i \sin \pi s$$

Therefore the sinusoidal components in the power spectra are caused by the Fourier transforms of delta functions. These features are compounded by shifting the delta functions further from the origin. From the shift theorem of Fourier transforms, if $f(x) \supset F(s)$ then $f(x - a) \supset e^{-i2\pi as}F(s)$. So the further the delta function is from the origin (large a), the higher the frequency of oscillations in the Fourier transform. The figures support the preceding argument. Figure 13a has delta functions at $N \simeq 120$ and $N \simeq 380$. Figure 12a has delta functions at $N \simeq 380$ and $N \simeq 950$. Consequently, the sinusoidal components in Figure 12b are of higher frequency than those in Figure 13b. The delta functions also cause more power to occur in the spectra (compare with Figure 11).

The ringing in the power spectra was eliminated by filtering the original data sets of data points which deviated significantly from the data set mean. The origin of the delta functions is probably instrumental.

Figure 12a: Atmosphere Stability Test Conducted on September 14, 1987

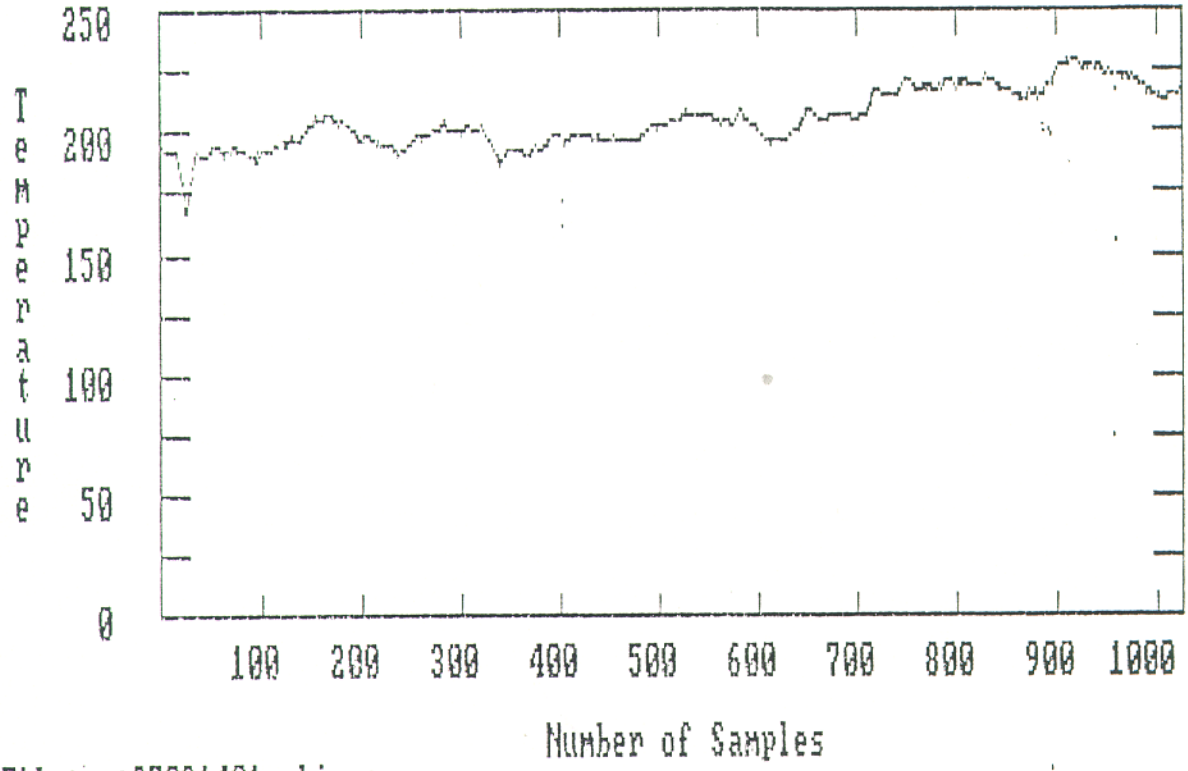

File: c:87091401.phi

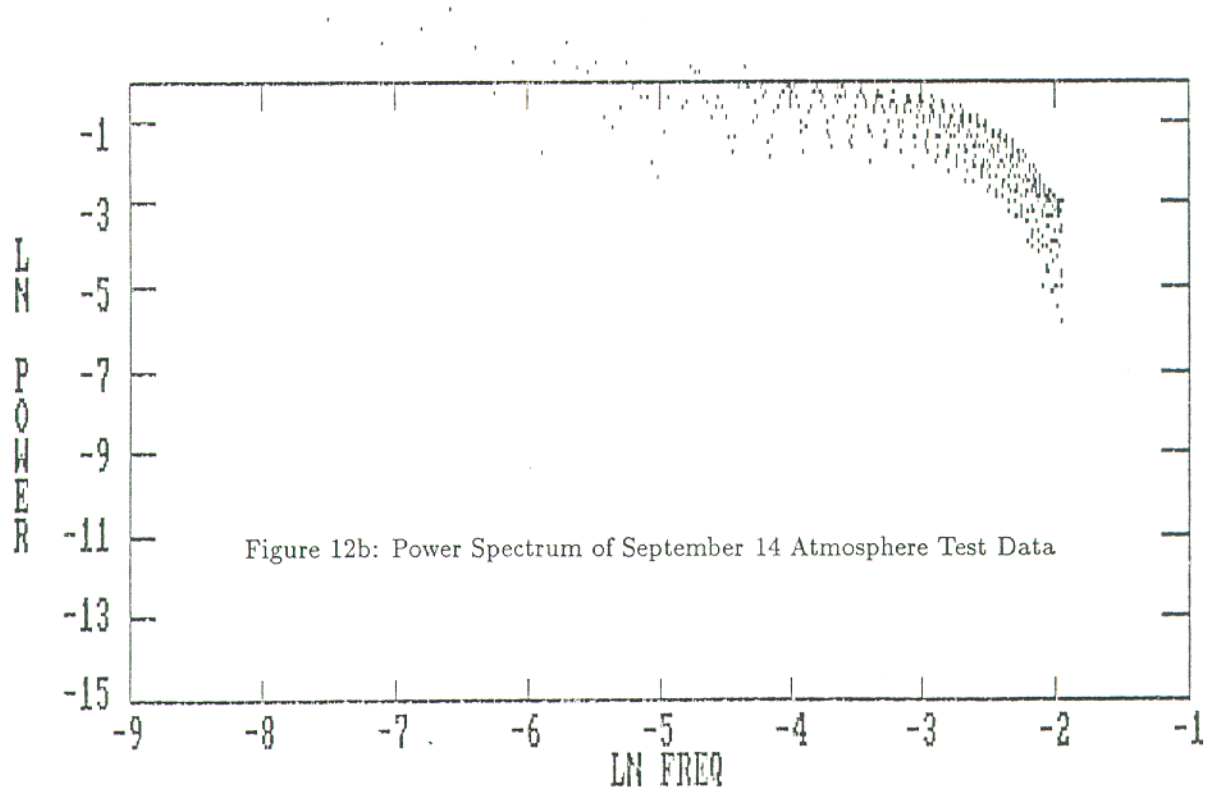

Figure 12b: Power Spectrum of September 14 Atmosphere Test Data

File: c:87091401.phi
slope = -0.953 +/- 0.037
intercept = -4.512 +/- 0.116
fit = -0.7

Figure 13a: Atmosphere Stability Test Conducted on September 15, 1987

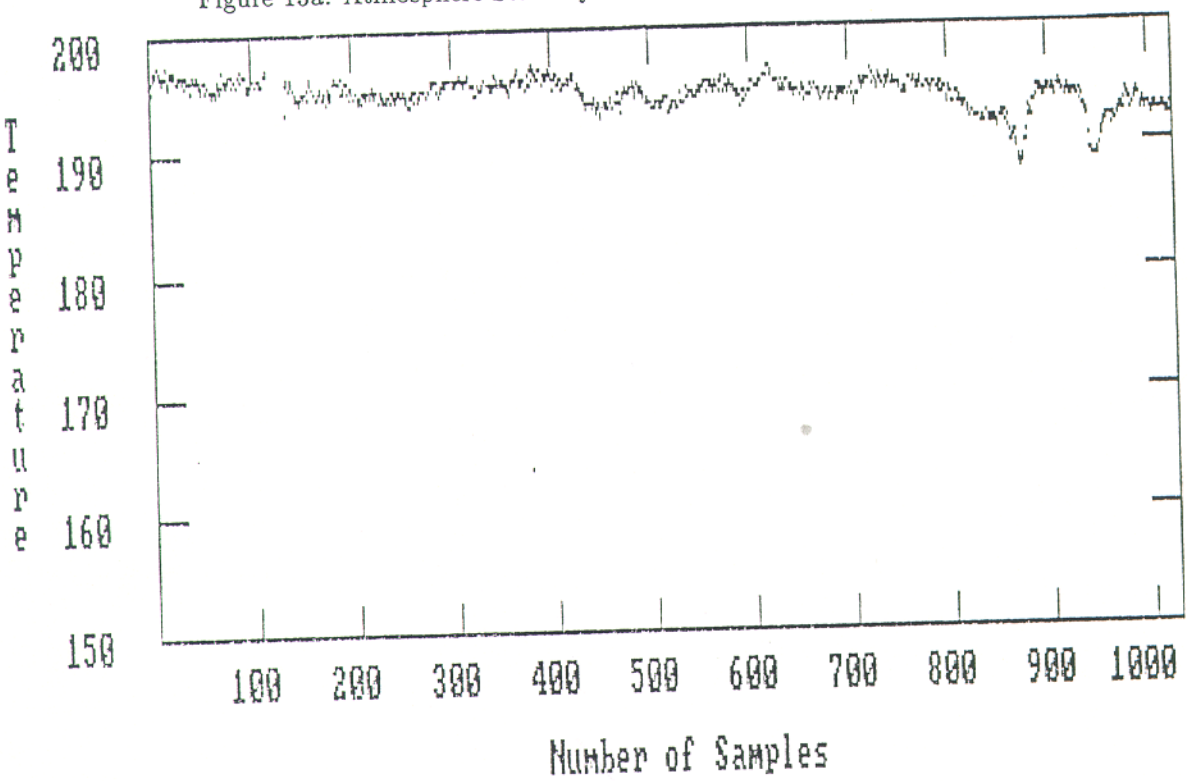

File: c:87091500.phi

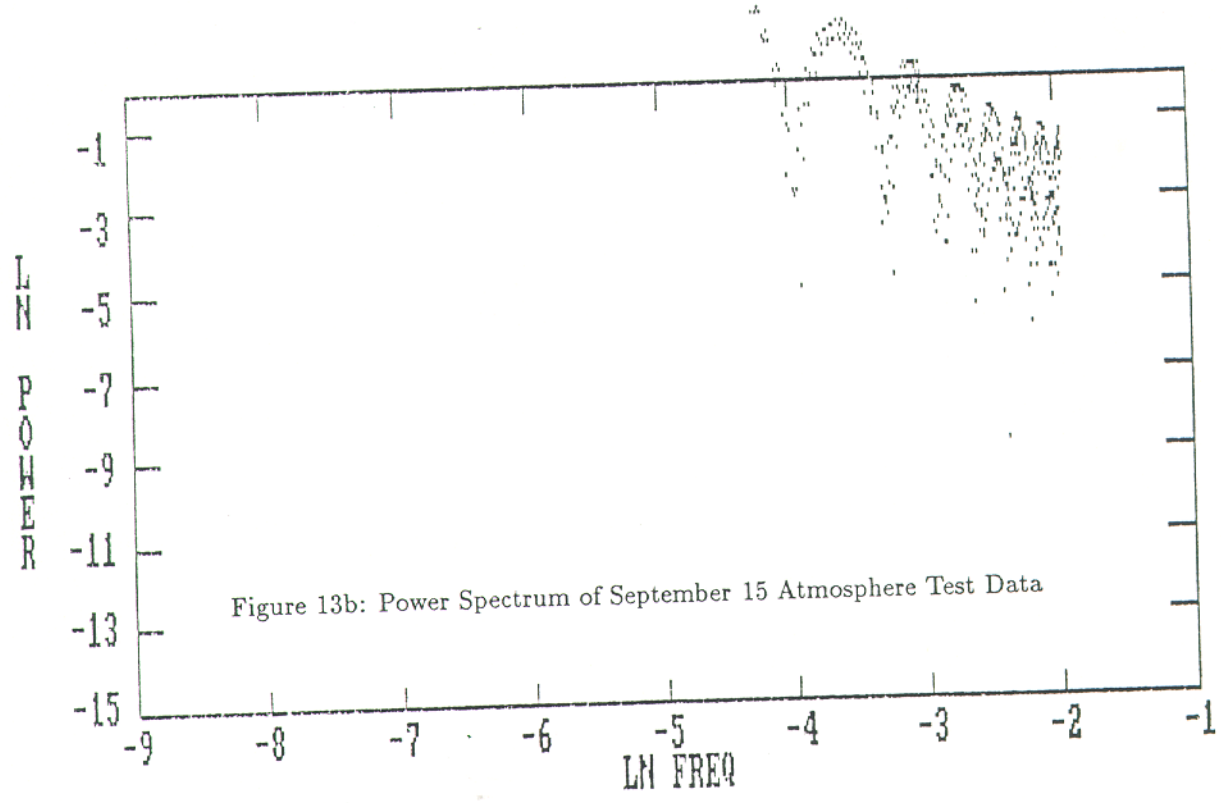

Figure 13b: Power Spectrum of September 15 Atmosphere Test Data

File: c:87091500.phi
slope = -1.840 +/- 0.055
intercept = -6.638 +/- 0.170
fit = -0.8

Appendix B: Computer Programs.

The following programs were written for a COMPAQ Portable personal computer with an 8087 math coprocessor in the language Turbo-Pascal.

PHITEST is the program which executes the radiometer phase stability runs and stores the time series data in a data file on disk.

VARYPHI is the program which reads and plots the time series data in the data file generated by PHITEST. Figure 1 is generated by VARYPHI.

The data stored by PHITEST is currently corrected for gain averaging with the program CONVERT. CONVERT writes a textfile containing the corrected data which may be accessed by the data analysis programs.

DFT 87 is the program which executes a discrete Fourier transform (DFT) on the time series data in the data file generated by CONVERT. The DFT is given by

$$F(\nu) = \frac{1}{N} \sum_{t=0}^{N-1} f(t) e^{i2\pi(\nu/N)t}.$$

DFT 87 computes power by summing the squares of the real and imaginary components of the Fourier transform. DFT 87 then plots the power spectrum, and calculates a spectral index by performing a least squares analysis. Figure 11 is generated by DFT 87.

ALLAN 87 is the program which calculates the Allan variance of the time series data in the data file generated by CONVERT. ALLAN 87 computes the Allan variance for time intervals of $\Delta t = 3.5 \times 2^n$ for $n = 0, 1, 2...8$. ALLAN 87 generates a log-log plot of Allan variance versus averaging time (Figure 8b).

The commercially available software package MATHCAD was used to perform a fast Fourier transform (FFT) on the time series data in the data file generated by PHITEST. The FFT in MATHCAD is much faster than the DFT in DFT 87 (two minutes versus 30 minutes). The MATHCAD output is shown in Figure 10a. Note that MATHCAD can read only text files. The current version of MATHCAD only allows 14 files to be opened with a single program. When the error message 'Too many files' appears, one must copy the original program to another file with the 'Append' command in MATHCAD. See the MATHCAD guide on how to use 'Append'.